NQO1 drives glioblastoma cell aggressiveness through EMT induction via the PI3K/Akt/mTOR/Snail pathway

LAN ZHENG[1-3*], SHIPENG YANG[1,4*], RAN XU[3,4], YANG YANG[3,4],
JISHU QUAN[4], ZHENHUA LIN[1,3,4] and CHUNHUA QUAN[1,3]

[1]Central Laboratory, Affiliated Hospital of Yanbian University, Yanji, Jilin 133002; [2]Department of Obstetrics and Gynecology,
Taizhou Hospital of Zhejiang Province Affiliated with Wenzhou Medical University, Linhai, Zhejiang 317000;
[3]Key Laboratory of Pathobiology, State Ethnic Affairs Commission, Yanbian University, Yanji, Jilin 133000;
[4]Department of Pathology, Yanbian University Medical College, Yanji, Jilin 133000, P.R. China

Abstract. Glioblastoma multiforme (GBM) is the most frequent and lethal cancer derived from the central nervous system, of which the mesenchymal (MES) subtype seriously influences the survival and prognosis of patients. NAD(P)H: quinone acceptor oxidoreductase 1 (NQO1) serves an important role in the carcinogenesis and progression of various types of cancer; however, the specific mechanism underlying the regulatory effects of NQO1 on GBM is unclear. Thus, the present study aimed to explore the role and mechanism of NQO1 in GBM progression. The results of bioinformatics analysis and immunohistochemistry showed that high expression of NQO1 was significantly related to the MES phenotype of GBM and shorter survival. In addition, MTT, colony formation, immunofluorescence and western blot analyses, and lung metastasis model experiments suggested that silencing NQO1 inhibited the proliferation and metastasis of GBM cells *in vitro* and *in vivo*. Furthermore, western blotting showed that the activity of the PI3K/Akt/mTOR signaling pathway was revealed to be inhibited by downregulation of NQO1 expression, whereas it was enhanced by overexpression of NQO1. Notably, co-immunoprecipitation and ubiquitination experiments suggested that Snail was considered an important downstream target of NQO1 in GBM cells. Snail knockdown could eliminate the promoting effect of ectopic NQO1 on the proliferation and invasion of GBM cells, and reduce its effects on the activity of PI3K/Akt/mTOR signaling pathway. These results indicated that NQO1 could promote GBM aggressiveness by activating the PI3K/Akt/mTOR signaling pathway in a Snail-dependent manner, and NQO1 and its relevant pathways may be considered novel targets for GBM therapy.

Introduction

Glioblastoma multiforme (GBM) is the most aggressive, highly heterogeneous and therapeutically challenging tumor of the brain (1,2). Although the possibility of distant metastasis is extremely rare, GBM is known to cause ventricular metastasis and cerebrospinal fluid dissemination forming aggressive secondary lesions resulting in a poor prognosis (3). Verhaak *et al* (4) proposed four molecular subtypes of GBM based on the different gene expressions: Proneural (PN), neural, classical and mesenchymal (MES) subtypes. Recent studies have suggested that MES is the most aggressive and the worst prognostic subtype in GBM (5,6). Additionally, the PN subtype of GBM is often accompanied by the MES subtype during radiation therapy and chemotherapy, enhancing the invasive capacity of the tumor (7).

At present, epithelial-to-MES transition (EMT) is usually described as a key mechanism, which can enable cancer cells to acquire MES properties and a more motile phenotype by losing cell polarity and intercellular adhesion, thus promoting the invasive and metastatic ability of cancer cells (8). As a key regulator of multiple signaling pathways leading to EMT, Snail is closely associated with GBM metastasis (9,10). Zhong *et al* (11) reported that LIM and SH3 protein 1 (LASP1) facilitates the invasion of glioma cells by activating the PI3K/AKT/Snail signaling pathway. A previous study also confirmed that microRNA-451 could reduce the EMT process and metastasis of glioma through inhibition of the PI3K/Akt/Snail signaling pathway (12). Therefore, it was hypothesized that blocking the PI3K/Akt/Snail pathway may significantly inhibit the EMT and metastasis of cancer cells in the treatment of the MES subtype of GBM.

NAD(P)H: quinone oxidoreductase 1 (NQO1) is located on chromosome 16q22 and is a widely distributed FAD-dependent flavoprotein, which was first discovered by Professor Ernster in 1958 (13). A previous study reported that C609T polymorphism

Correspondence to: Professor Chunhua Quan, Central Laboratory, Affiliated Hospital of Yanbian University, 1327 Juzi Street, Yanji, Jilin 133000, P.R. China
Email: 9000002277@ybu.edu.cn

*Contributed equally

of the NQO1 gene is related to tumor susceptibility, inhibition of NQO1 detoxification and cytoprotection (14). Our previous studies showed that NQO1 is significantly upregulated in various types of solid cancer compared with in adjacent normal tissues, such as breast cancer, pancreatic cancer, lung cancer and hepatocellular carcinoma, and its high expression is closely related to the poor prognosis of patients with cancer (15-17). Furthermore, a previous study demonstrated that depleting NQO1 expression can suppress cell proliferation and decrease lung tumor xenograft growth (18). Yang *et al* (19) reported that NQO1 significantly affected the growth and aggressiveness of breast cancer by modulating pyruvate kinase L/R. Moreover, Thapa *et al* (20) showed that NQO1 can regulate the transforming growth factor-β (TGF-β) signaling pathway to curb EMT and migration, which are necessary for prostate cancer progression. Shimokawa *et al* (21) suggested that modulation of NQO1 activity intercepts anoikis resistance and reduces the metastatic potential of hepatocellular carcinoma. All of these reports indicated that NQO1 may serve vital roles in the metastasis of multiple types of cancer; however, its specific mechanism in the MES subtype of GBM remains unclear. The present study aimed to investigate the function of NQO1 in the MES subtype of GBM progression, to uncover its underlying mechanism, and to provide insights into the development of more efficient regimens for the MES subtype of GBM treatment.

Materials and methods

Clinical samples. A glioma tissue microarray was purchased from Shanghai Outdo Biotech Co., Ltd., including 195 cases of glioma tissue and 17 cases of normal cancer-adjacent tissue. The use of the glioma tissue microarray was approved by the Ethics Committee of Yanbian University Medical College (Yanji, China) (approval no. YD20230406015). The histological grade of GBM tumors was evaluated, according to the World Health Organization (WHO) criteria (22).

Cell culture. The U87 human GBM of unknown origin cell line (HTB-14™) is a cell line with epithelial morphology that was isolated from the malignant glioma of a male patient who likely had GBM. U87 cells, the GBM cell lines T98G (CRL-1690) and SHG44, and the 293T cell line were all purchased from American Type Culture Collection in 2020. The U251 GBM cell line was purchased from The National Collection of Authenticated Cell Cultures in 2020. The normal human astrocytes (NHAs; primary cells; cat. no. CC-2565; Lonza Group, Ltd.) were purchased in 2020. The SHG66 primary human malignant glioma cell line (isolated from the brain tissue of a 47-year-old male patient with grade IV glioma from China) was obtained from the Department of Neurosurgery, Huashan Hospital, Fudan University (Shanghai, China). All cell lines were authenticated and characterized by the supplier. The need for ethics approval for the use of commercial primary cell lines was waived by the Medical Ethics Committee of Yanbian University Medical College. Cells were used within 6 months of resuscitation, were confirmed to be mycoplasma-free and were routinely authenticated by quality examinations of morphology and growth profile. All cell lines were cultured in Dulbecco's modified Eagle's medium

containing 10% fetal bovine serum (both from Gibco; Thermo Fisher Scientific, Inc.) and penicillin-streptomycin (100 U/ml) at 37 °C and 5% CO_2.

Antibodies. Antibodies against E-cadherin (cat. no. ab40772) and Vimentin (cat. no. ab92547) were purchased from Abcam. Antibodies against Slug (cat. no. #9585), twist-related protein (Twist; cat. no. #90445), p27 (cat. no. #3686), Cyclin B (cat. no. #4138), Cyclin D (cat. no. #55506), cyclin-dependent kinase 1 (CDK1; cat. no. #77055), eIF4E-binding protein (4EBP1; cat. no. #9644), phosphorylated (p)-4EBP1 (cat. no. #2855), p-ribosomal protein S6 (S6; cat. no. #4858), S6 (cat. no. #2317), p-Akt (cat. no. #4060), Akt (cat. no. #9272), p-PI3K (cat. no. #17366), PI3K (cat. no. #4255), p-mammalian target of rapamycin (mTOR; cat. no. #2971), mTOR (cat. no. #2972) and β-actin (cat. no. #93473) were purchased from Cell Signaling Technology, Inc. Antibodies against Ki67 (cat. no. 27309) and Snail (cat. no. 13099) were purchased from Proteintech Group, Inc. The antibody against NQO1 (cat. no. sc-32793) was purchased from Santa Cruz Biotechnology, Inc.

Small interfering RNA (siRNA) transfection. Snail siRNAs [si-control (non-targeting sequence), siRNA1, siRNA2 and siRNA3] were purchased from Guangzhou RiboBio Co., Ltd. The siRNA sequences are presented in Table SI. T98G, SHG44, and NQO1-overexpressing T98G and SHG44 cells ($5x10^5$ cells/well) were transfected with si-control (5 nmol; cat. no. siN0000001-1-5), siRNA1 (5 nmol; cat. no. stB0002558A-1-5), siRNA2 (5 nmol; cat. no. stB0002558B-1-5) and siRNA3 (5 nmol; cat. no. stB0002558C-1-5) in 6-well plates using Lipofectamine® 3000 (Invitrogen; Thermo Fisher Scientific, Inc.) according to the manufacturer's protocol at 37°C for 6 h. The time interval between transfection and subsequent experimentation was 48 h.

Stable cell line generation. U87, SHG66, T98G and SHGs44 cells were counted and inoculated in 6-well plates (~$1x10^5$ cells/well). Transfection was performed when the cells were in a suitable condition (the cells were complete, homogeneous, transparent and with few particles; the culture medium was clear and transparent, without suspended cells and fragments) and without antibiotics. The pLV[shRNA]-EGFP/Puro-U6-Scramble-shRNA (sh-Con), pLV[shRNA]-EGFP: T2A: Puro-U6-{hNQO1[shRNA#1]} (sh-NQO1), empty vector pLV[Exp]-EGFP: T2A: Puro-Null (vector) and pLV[Exp]-EGFP: T2A: Puro-hNQO1[NM-000903.2] (NQO1) lentiviral plasmids were purchased from Cyagen Biosciences, Inc. Briefly, 4 μg Human Lenti-shNQO1-green fluorescent protein (GFP; sh-NQO1), Lenti-NQO1-GFP (NQO1) and their controls (empty vector and sh-Con) were packaged (10 μg overexpression plasmid or 0.1-0.2 μg shRNA plasmid, 6.5 μg packaging plasmids and 3.5 μg envelope plasmids) in 293T cells for 48 h in a 37°C incubator. The U87, SHG66, T98G and SHG44 cells were cultured at $1x10^5$ cells/well into 6-well tissue culture plates at 37°C overnight. The lentiviral supernatant was added into cells and the multiplicity of infection was 10 at 37°C for 48 h. After transduction, cells were selected with 2 μg/ml puromycin

(MilliporeSigma) to generate stable cell lines at 37˚C for 2 weeks. Subsequently, the cells were maintained in complete medium with puromycin at a concentration of 0.5 μg/ml and collected for western blotting, MTT assays, EdU assays and colony formation assays 48 h post-transduction.

Wound healing assay. The U87, SHG66, T98G and SHG44 cells were routinely digested and placed in a 6-well plate, and cell wounds were created by scratching cells using a micropipette tip when cell confluence reached 90-100% after cell adhesion. The medium was discarded and the cells were washed with 1X PBS three times to remove floating cells, followed by the addition of serum-free medium. Spontaneous cell migration was monitored using a Nikon inverted light microscope (Nikon Corporation) at 0, 24 and 48 h. The occupancy of wound area (%) was calculated by measuring the width of the wound as follows: Occupancy of wound area (%)=(24/48 h occupancy of wound area)/0 h occupancy of wound area x100. Wound closure distance was measured for three independent wounds in each group using ImageJ (v1.53e) software (National Institutes of Health).

Immunofluorescence (IF). The U87, SHG66, T98G and SHG44 cells were grown in glass-covered six-well plates until they reached 90% confluence. The cells were washed with PBS at room temperature for 15 min, and fixed with 4% paraformaldehyde at room temperature for 15 min, permeabilized with 0.5% Triton X-100 (CWBio) and blocked with 3% BSA (CAS:9048-46-8; Beijing Solarbio Science & Technology Co., Ltd.) at room temperature for 2 h. The cells were incubated with primary antibodies against E-cadherin (1:400), Vimentin (1:400), Snail (1:200) and NQO1 (1:400) at 4˚C overnight, washed with PBS three times, and then incubated for 2 h with Alexa Fluor® 488-conjugated secondary antibody (cat. no. A31627; 1:400; Invitrogen; Thermo Fisher Scientific, Inc.). Finally, the cells were analyzed under a Leica SP5II confocal microscope (Leica Microsystems, Inc.).

Cell invasion and migration assays. Cell invasion and migration assays were performed in 24-well, two-chamber plates with high-throughput screening multiwell inserts (Becton, Dickinson and Company), which contain polycarbonate filters (pore size, 8 μm). For cell invasion, $5x10^4$ cells were added to the upper chamber, which was coated in Matrigel at room temperature for 12 h, medium with fibronectin (20 μg/ml; MFCD00131062; Sigma-Aldrich; Merck KgaA) was added to the lower chamber, and the cells were incubated at 37˚C for 30 h. For cell migration, $3x10^4$ cells were added to the upper chamber, medium without fibronectin was added to the lower chamber, and the cells were incubated at 37˚C for 24 h. Invaded or migrated cells (on the lower side of the membranes or in the lower well) were then fixed in 100% methanol for 30 min and stained with gentian violet solution at room temperature for 10 min. Cells were counted under a light microscope (BX53; Olympus Corporation) at x200 magnification. Each assay was performed in duplicate and repeated three times.

MTT. The U87, SHG66, T98G and SHG44 cellswere seeded at a concentration of $1x10^4$ cells/well in 96-well plates. After cell adhesion, MTT solution (1 mg/ml; 100 μl/well) was added and the cells were cultured for 4 h. MTT solution was removed and 100 μl dimethyl sulfoxide was then added to each well and agitated for 10 min at room temperature, away from the light. Subsequently, the optical density was measured at 550 nm using an ELISA plate reader.

Colony formation assay. The U87, SHG66, T98G and SHG44 cells were seeded in 12-well plates at a density of $1x10^3$ cells/well in human methylcellulose complete medium (R&D Systems Europe, Ltd.) according to the manufacturer's instructions. Culture medium was replaced every 3 days. After 14 days of incubation at 37˚C and 5% CO_2, PBS was used to wash the cells before fixing them with pre-cooled (1:1) methanol/acetone at -20˚C for 15 min. After staining with 1% crystal violet for 15 min at room temperature, colonies containing ≥50 cells were counted using an inverted light microscope (magnification, x200; CKX41; Olympus Corporation).

EdU assay. EdU is a thymine nucleoside analogue. EdU, instead of thymidine, can be inserted into the replicating DNA molecules during cell proliferation, marking the newly synthesized DNA with Apollo fluorescent dye-containing EdU. The Cell-Light™ EdU Apollo®488 *In Vitro* Imaging Kit (Guangzhou RiboBio Co., Ltd.) was performed according to the manufacturer's instructions. Cells ($5x10^3$/well) were seeded and grown in 96-well plates overnight, 50 μM EdU medium (1:1,000) was added to each well and cells were cultured at 37˚C for 2 h. Subsequently, the cells were fixed with methanol for 30 min and washed twice with PBS for 5 min at room temperature. After permeabilizing with 0.5% Triton X-100 for 10 min twice and washing with PBS at room temperature for 5 min, 1X Apollo dye was used to stain the cells at room temperature for 30 min, and the cells were washed again. Finally, the signal was visualized and recorded using a Leica SP5II confocal microscope after Hoechst 33342 counterstaining for 10 min in the dark.

Western blotting. Western blot analysis was performed according to standard methods. Briefly, cell lysis and protein extraction were performed using RIPA buffer (cat. no. CW2333S; CWBIO). The protein concentration was measured using a BCA Protein Assay Kit (Beijing Solarbio Science & Technology Co., Ltd.). Subsequently, the proteins (30 μg/lane) were separated by SDS-PAGE electrophoresis on 8-12% polyacrylamide gels and were transferred to PVDF membranes (MilliporeSigma). After blocking with 5% non-fat milk at room temperature for 2 h, the membrane was incubated overnight at 4˚C with primary antibodies against E-cadherin (1:1,000), Vimentin (1:1,000), Slug (1:1,000), Twist (1:1,000), p27 (1:1,000), CDK1 (1:1,000), Cyclin B (1:1,000), Cyclin D (1:1,000), CDK1 (1:1,000), 4EBP1 (1:1,000), p-4EBP1 (1:1,000), p-S6 (1:1,000), S6 (1:1,000), p-Akt (1:1,000), Akt (1:1,000), p-PI3K (1:1,000), PI3K (1:1,000), p-mTOR (1:1,000), mTOR (1:1,000), β-actin (1:3,000), Snail (1:1,000) and NQO1 (1:1,000). Membranes were then washed with TBS-0.1% Tween, and incubated with goat anti-rabbit IgG (H&L) secondary antibodies (1:10,000; cat. no. bs13278; Bioworld Technology, Inc.) or goat anti-mouse IgG (H&L) secondary antibodies (1:10,000; cat. no. bs12478; Bioworld Technology, Inc.) at 25˚C for 1 h. The protein bands were visualized using

an Amersham Imager 680 (Cytiva) with enhanced chemi-luminesence (cat. no. WBKLS0500; MilliporeSigma). The relative expression of each protein was calculated using ImageJ (version 1.8.0.345) with β-actin as an internal reference.

In vivo tumorigenesis and metastasis assays. A total of 32 BALB/c nude mice (male; age, 4-5 weeks; weight, 18-20 g) were purchased from the Beijing Vital River Laboratory Animal Technology Co., Ltd. BALB/c nude mice (four per cage) were housed under specific pathogen-free conditions (temperature, 21±8˚C; humidity, 40-60%; 12-h light/dark cycle; free access to standard sterile food and water) and were ear-notched for identification. To assess the effect of NQO1 on tumorigenicity *in vivo* (n=16 mice), U87 cells ($3x10^6$ cells transduced with sh-Con or shNQO1) and SHG44 cells ($3x10^6$ cells transduced with Vector or NQO1) were injected subcutaneously into the left dorsal of nude mice to construct a subcutaneous tumor-forming model of nude mice.

To establish the lung metastasis model in another 16 BALB/c nude mice (male; age, 4-5 weeks; weight, 18-20 g), U87 cells transduced with sh-Con or shNQO1 (0.1 ml, $1x10^6$ cells/mouse; four mice/group), and SHG44 cells transduced with Vector or NQO1 (0.1 ml, $1x10^6$ cells/mouse; four mice/group), were intravenously injected into the tail vein of nude mice using a 28-gauge syringe. The tumor volume (mm^3) in each mouse was measured using a Vernier caliper every 3 days and was calculated as follows: Tumor volume=0.5 x length x width^2. Mice were euthanized after 21 days for the xenograft study and after 8 weeks for the lung metastasis experiment.

To assess the effect of NQO1 on tumorigenicity *in vivo* (intracranial xenograft model), U87 cells transduced with sh-con or shNQO1 ($2x10^5$ cells) were injected stereotacti-cally into the right hemicerebrum of 4-6-week-old female nude mice (n=11; NOD-SCID; Cyagen Biosciences, Inc.). These mice were housed under the same conditions as the BALB/c nude mice. Tumor growth was monitored using an *in vivo* imaging system (IVIS Lumina II; PerkinElmer, Inc.). The tumors were excised on day 15 after the injection. The following humane endpoints were established: Tumor diameter, >2.0 cm; weight loss >20%; poor overall condition (22). None of the mice reached the humane endpoints in the present study. To reduce suffering, mice were anesthetized with 2% isoflurane. All mice were then rapidly euthanized by cervical dislocation. Verification of death included cardiac and respiratory arrest, lack of reflexes and changes in mucosal color. After subcutaneous tumors were dissected, they were weighed using a digital balance (Mettler Toledo), fixed with 4% formalin (Biosharp Life Sciences) at room temperature for 24 h and embedded with paraffin to prepare sections. Further immuno-histochemical staining was performed to detect the expression levels of Vimentin, E-cadherin and Ki67 in xenograft tissue sections. No metastatic nodules were found in the abdominal and thoracic organs of the subcutaneous xenograft mice. After verification of death, lungs were completely dissected from the lung metastasis model mice. The lungs were fixed with 4% formalin at room temperature for 24 h, embedded in paraffin, cut into sections (5 µm) and stained with hematoxylin-eosin (H&E) for histopathological evaluation. The sections were dewaxed in dimethylbenzene for 5 min, and dehydrated in 100, 95, 85 and 75% alcohol for 5 min, respectively.

Subsequently, the sections were stained with hematoxylin for 5 min and differentiated with 1% hydrochloric acid alcohol for 5 sec. Sections were then stained with eosin for 15 sec and dehydrated in 95 and 100% alcohol for 1 min each, before clearing with dimethylbenzene for 5 min. Subsequently, the sections were fixed using neutral balsam. All stages of H&E staining were performed at room temperature. Metastatic lung nodules were counted using a light microscope (IX51; Olympus Corporation). All experiments were performed in accordance with the procedures and protocols of the Animal Ethics Committee of Yanbian University.

Immunohistochemistry (IHC). Tissue sections (glioma tissue microarray and xenograft tissues collected from animal models) were washed with normal saline and immediately fixed in 4% paraformaldehyde at room temperature for 24 h. Paraffin-embedded tissues were then cut into 5-µm sections, were dewaxed at 58˚C, then incubated in dimethylbenzene for 10 min, 100% alcohol for 5 min, 95% alcohol for 5 min and 75% alcohol for 5 min at room temperature for rehydration. The sections were then washed with water and antigen retrieval was performed using boiling EDTA for 15 min. The tissue sections were soaked in 3% H_2O_2 at room temperature for 30 min. Subsequently, the sections were washed another three times with PBS and were incubated at 37˚C overnight with the following primary antibodies: E-cadherin (1:200) and Vimentin (1:200), Ki67 (1:200) and NQO1 (1:200). Sections were then rinsed with PBS, rinsed three times with water, and soaked and rinsed in PBS-10% Tween three times, before being incubated with goat anti-rabbit IgG (H&L) secondary antibodies (1:2,000; cat. no. ab205718; Abcam) for 45 min at 37˚C. Subsequently, DAB was added to allow the assessment of color development under a microscope. After color development, the reaction was terminated with water and the sections were soaked. Hematoxylin dye solution was then added at room temperature for 2 min, the sections were rinsed with distilled water and color separation solution (cat. no. BSBA-4027; OriGene Technologies, Inc.) was added, after which the sections were rinsed with water a further three times. The slides were sequentially dehydrated in 100% absolute ethanol at 25˚C for 10 sec and a charge-coupled device light microscope was used for the assessment and imaging of sections.

All tissue specimens were examined and scored by two pathologists using a double-blind control method. Immunohistochemical analysis was performed using a semi-quantitative scoring system, which combined positive area percentage and staining intensity. NQO1-, Vimentin- and E-cadherin-positive staining intensity scores were as follows: negative, 0; weak, 1; medium, 2; strong, 3. The percentage of stained cells was scored as follows: ≤25%, 1; 26-50%, 2; 51-75%, 3; >75%, 4. The staining index was calculated by multiplying the staining intensity score with the percentage of positive staining score (value 0-12). NQO1, Vimentin and E-cadherin immunostaining values 0-3 were defined as low expression, whereas ≥4 was defined as high expression.

Bioinformatics analysis. Tumor Immune Estimation Resource (TIMER) (https://cistrome.shinyapps.io/timer/), University of California Santa Cruz (UCSC) (https://xenabrowser.net/),

University of ALabama at Birmingham Cancer (UALCAN) (http://ualcan.path.uab.edu), Gene Set Co-Expression Analysis (GSCA) (http://bioinfo.life.hust.edu.cn/GSCA/#/), TISIDB (an integrated repository portal for tumor-immune system interactions) (http://cis.hku.hk/TISIDB/), The Cancer Genome Atlas (TCGA) (https://www.cancer.gov/ccg/research/genome-sequencing/tcga) and Gene Expression Profiling Interactive Analysis (GEPIA) (gepia.cancer-pku.cn) were used to explore NQO1 expression in pan-cancer. ENCORI (http://starbase.sysu.edu.cn/index.php), Gene Expression Omnibus (https://www.ncbi.nlm.nih.gov/geoprofiles/) and Oncomine (https://www.oncomine.org/resource/main.html) were used to analyze the differential expression of NQO1 in GBM tissues and adjacent normal tissues. The relationship between NQO1 expression and patient survival was searched in Kaplan-Meier Plotter (http://kmplot.com/anaLysis/index.php?p=service) and UALCAN. LinkedOmics (http://www.linkedomics.org/login.php), cBioPortal (http://www.cbioportal.org), ChIPBase v3.0 (https://rnasysu.com/chipbase3/index.php) and TIMER databases were used to explore genetic Pearson correlation analysis.

Co-immunoprecipitation (Co-IP) and detection of ubiquitylation. Co-IP was performed with IgG (1:1,000; cat. no. sc-2025; Santa Cruz Biotechnology, Inc.) anti-NQO1 (1:1,000; cat. no. sc-32793; Santa Cruz Biotechnology, Inc.) and anti-Snail (1:1,000; cat. no. 13099-1-AP; Proteintech Group, Inc.) antibodies using the Protein A/G PLUS-Agarose (cat. no. sc-2003; Santa Cruz Biotechnology, Inc.) and IP/Co-IP kit (cat. no. ab206996; Abcam) according to the manufacturer's protocol. The kit contained Protein A/G magnetic beads, lysis/wash buffer, SDS-PAGE protein loading buffer (5X), elution buffer and neutralization buffer. Briefly, lysis/wash buffer and PMSF (1:100, cat. no. P0100; Beijing Solarbio Science & Technology Co., Ltd.) were added at a ratio of 30 μl per $1.0x10^5$ cells, mixed well and incubated on ice for 30 min (mixing several times during this period). Subsequently, this mixture underwent centrifugation (4°C; 12,000 x g; 10 min) with the supernatant placed on ice for later use. The prepared sample (500 μl) was added to a 1.5 ml Eppendorf (EP) tube, followed by 4 μg antibody and incubated on a flip mixer (4°C overnight) to form antigen-antibody complexes. The magnetic bead suspension (25 μl) was placed into a 1.5 ml EP tube and 500 μl lysis/wash buffer was added; the magnetic beads were resuspended by gently pipetting and then left to stand on a magnetic stand for 1 min. When the magnetic beads were adsorbed to the sides of the EP tube, the supernatant was aspirated and this step was repeated twice. The antigen-antibody complex was added to the pretreated magnetic beads and incubated on an inversion mixer at 4°C overnight before being left to stand on the magnetic stand for 1 min, until the magnetic beads were adsorbed to the sides of the EP tube. The supernatant was then aspirated and discarded; what remained in the tube was the antigen-antibody-magnetic bead complex. Lysis/rinse buffer (500 μl) was added to the antigen-antibody-magnetic bead complex, the magnetic beads were resuspended by gently pipetting and agitating, and was then allowed to stand on a magnetic stand for 1 min until the magnetic beads were adsorbed to the sides of the tube. The supernatant was aspirated and discarded and this step was repeated twice. An appropriate amount of 5X SDS-PAGE loading buffer was added to the antigen-antibody-magnetic bead complex, mixed well and heated at 100°C for 10 min. After cooling, the EP tube was placed on a magnetic stand for 1 min. After the magnetic beads were adsorbed to the sides of the EP tube, the supernatant was collected and detected by western blotting as aforementioned. For ubiquitylation, cells were treated with or without MG132 (10 μM; S2619; Selleck Chemicals) at 4°C for 6 h before being harvested in IP lysis buffer, followed by the aforementioned co-IP and western blotting protocols. In addition, ubiquitin (1:1,000; cat. no. sc-8017; Santa Cruz Biotechnology, Inc.) was detected by western blotting.

Rescue experiments. Rescue experiments were used to clarify whether NQO1 could induce the malignant evolution of GBM by activating the PI3K/Akt/mTOR signaling pathway. For rescue experiments, the cells were divided into the following four groups: Vector, NQO1, NQO1 + LY294002 (50 μM; cat. no. S1105; Selleck Chemicals; treated at 37°C for 48 h,) and NQO1 + Rapamycin (50 nM; cat. no. S1039; Selleck Chemicals; treated at 37°C for 48 h). The NQO1 group acted as the control. Subsequent experiments included MTT, EdU, colony formation, wound healing and cell migration assays, IF and western blotting.

Statistical analysis. Data were collected from three independent experiments. Statistical analysis was performed using SPSS 20.0 software (IBM Corp.), GraphPad Prism 8.0 software (Dotmatics), ImageJ software (v1.53e) and R software (version 3.5.2; portable version, https://www.r-project.org/). Statistical differences between two groups were determined using an unpaired t-test, whereas those between multiple groups were determined using a one-way ANOVA followed by Bonferroni test post hoc test. Semi-quantification of the cell number, colony number, wound gap closure and western blotting band integrated density were performed using ImageJ software. The χ^2 test was used to determine the relationship between NQO1 protein expression and clinicopathological parameters. Kaplan-Meier method was used to generate survival curves and log-rank test was used to determine P-values; the Renyi test was performed to determine the P-values when survival curves crossed over. Cox proportional hazards models were applied to evaluate the hazard ratios (HR) in univariate and multivariate logistic regression analyses. Receiver operating characteristic (ROC) curve analysis was applied to evaluate the diagnostic value of NQO1 in GBM. $P < 0.05$ was considered to indicate a statistically significant difference.

Results

NQO1 is generally highly expressed in cancer and predicts a poor prognosis. All four databases (TIMER1, UCSC, GEPIA and TCGA) showed that NQO1 mRNA expression was significantly increased in the tumor tissues of digestive, respiratory and female reproductive system cancer compared with that in unpaired normal tissues (Fig. 1A-D). Based on the UALCAN portal, it was revealed that NQO1 protein expression was increased in various cancer types, including colon cancer,
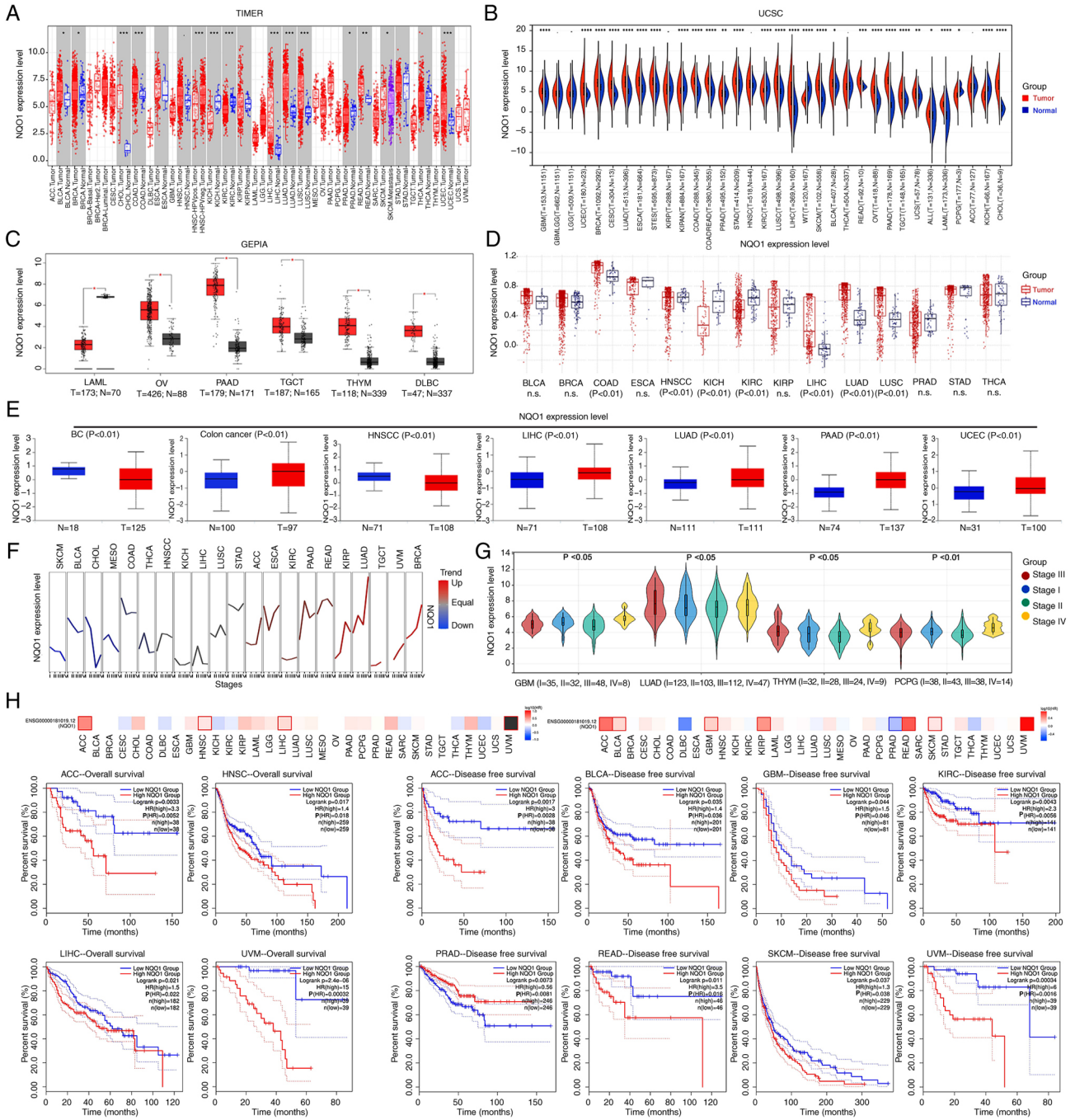
Figure 1. Expression of NQO1 in pan-cancer. mRNA expression levels of NQO1 in normal and tumor tissues were analyzed using (A) TIMER, (B) UCSC, (C) GEPIA and (D) TCGA databases. (E) Protein expression levels of NQO1 in normal and tumor tissues were analyzed using CTPAC database. The expression of NQO1 in different cancer stages was analyzed using (F) GSCA and (G) UCSC databases. (H) Overall survival and disease-free survival of patients with cancer split according to NQO1 expression were detected using the GEPIA database. n.s., P>0.05, *P<0.05, **P<0.01, ***P<0.001, ****P<0.0001. NQO1, NAD(P)H:quinone acceptor oxidoreductase 1; TIMER, Tumor Immune Estimation Resource; UCSC, University of California Santa Cruz; GSCA, Gene Set Co-Expression Analysis; UALCAN, University of ALabama at Birmingham Cancer; TCGA, The Cancer Genome Atlas; GEPIA, Gene Expression Profiling Interactive Analysis.

liver hepatocellular carcinoma (LIHC), lung adenocarcinoma, pancreatic adenocarcinoma and uterine corpus endometrial carcinoma, but its expression was decreased in breast cancer (BC), and head and neck squamous cell carcinoma (HNSCC) (Fig. 1E). Subsequently, the GSCA database revealed that the expression levels of NQO1 were significantly related with the stages of certain cancer types, such as lung adenocarcinoma and breast cancer (Fig. 1F). Since the GSCA does not currently include some cancer types, the relationship between NQO1

mRNA expression and cancer stage was analyzed in the UCSC database instead. The results showed that the mRNA expression of NQO1 was relevant to the stage of GBM, thymoma, and pheochromocytoma and paraganglioma (Fig. 1G). Moreover, the overall survival of patients with high NQO1 expression was much lower than that of patients with low NQO1 expression in adrenocortical carcinoma (ACC), LIHC and uveal melanoma (UVM) (Fig. 1H). Similarly, the disease-free survival of patients with high NQO1 expression was significantly shorter
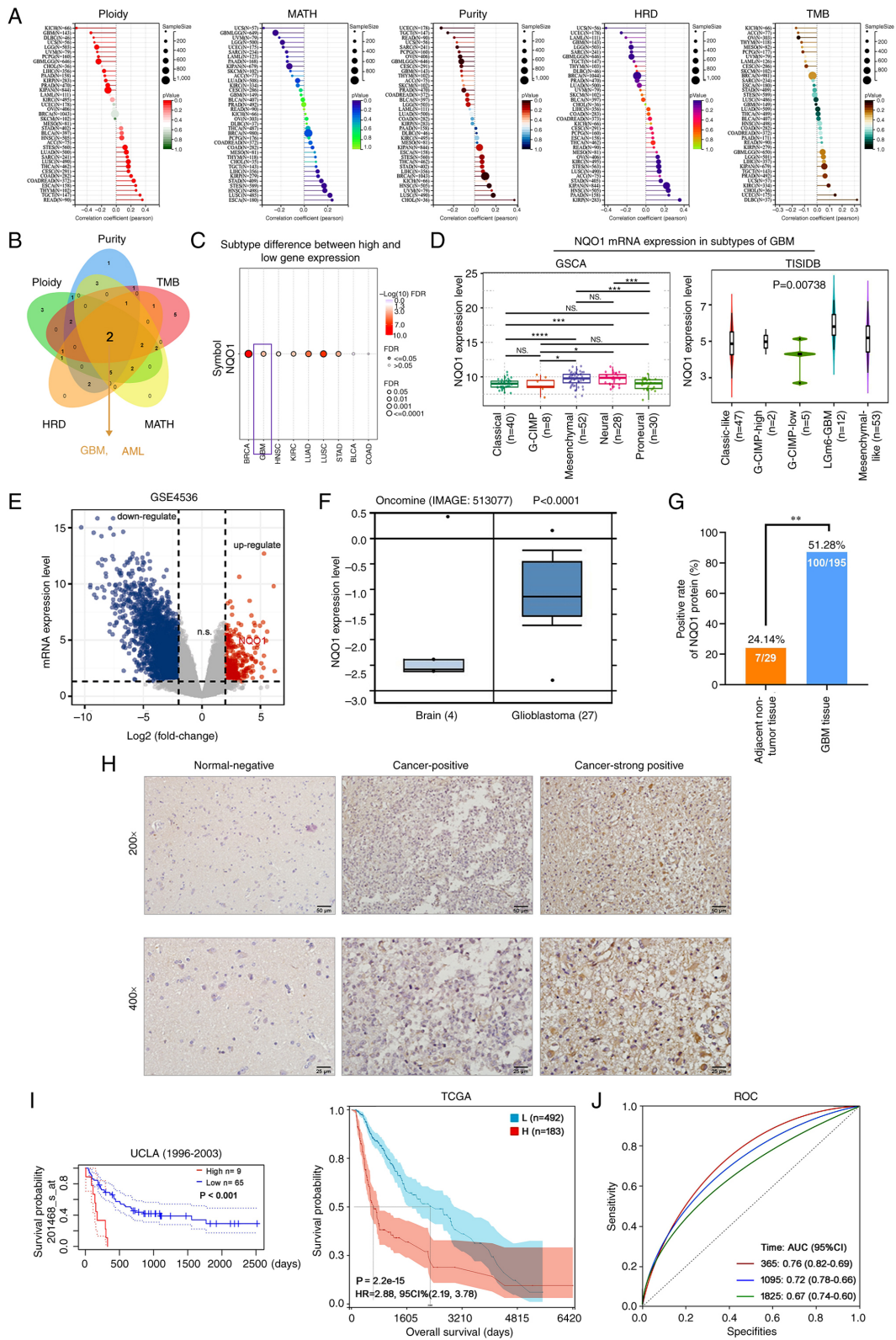
Figure 2. NQO1 expression is upregulated and associated with poor outcome in patients with GBM. (A) Correlation between NQO1 expression level and ploidy, MATH, purity, HRD and TMB were analyzed using TCGA database. (B) Intersection analysis of NQO1 and ploidy, MATH, purity, HRD and TMB was determined using a Venn diagram. (C) Correlation between NQO1 and cancer subtype was assessed using the GSCA database. (D) mRNA expression levels of NQO1 in GBM subtypes were assessed using GSCA and TISIDB databases. (E) The mRNA expressions of differentially expressed genes in GBM were analysed by using GEO database. (F) mRNA expression levels of NQO1 were assessed using the Oncomine database in brain and GBM tissues. (G) Positive rate of NQO1 protein expression in adjacent non-tumor (n=29) and GBM (n=195) tissues. (H) Representative images of immunohistochemistry staining of the tissue microarray from patients with GBM. Scale bars, upper: 50 μm; lower: 25 μm. (I) Kaplan-Meier survival analysis of patients with GBM and low or high NQO1 expression in UALCAN and TCGA databases. (J) Diagnostic value of NQO1 in patients with GBM was determined using ROC curve analysis. [*]P<0.05, [**]P<0.01, [***]P<0.001, [****]P<0.0001. NQO1, NAD(P)H:quinone acceptor oxidoreductase 1; MATH, mutant-allele tumor heterogeneity; HRD, homologous recombination deficiency; TMB, tumor mutational burden; GBM, glioblastoma multiforme; ROC, receiver operating characteristic; UALCAN, University of ALabama at Birmingham Cancer; TCGA, The Cancer Genome Atlas; TISIDB, an integrated repository portal for tumor-immune system interactions; GSCA, Gene Set Co-Expression Analysis.

Table I. Association of NQO1 expression with clinicopathological characteristics in GBM.

Feature	N	NQO1 expression High (%)	NQO1 expression Low (%)	χ^2	P-value
Sex					
Male	132	66 (50.0)	66 (50.0)	0.269	0.604
Female	63	34 (54.0)	29 (46.0)		
Age, years					
<50	100	49 (49.0)	51 (51.0)	0.428	0.513
≥50	95	51 (53.7)	44 (46.3)		
Tumor size, cm					
<4	70	35 (50.0)	35 (50.0)	0.072	0.789
≥4	125	65 (52.0)	60 (48.0)		
Tumor location					
Left	82	45 (54.9)	37 (45.1)	1.331	0.514
Right	89	45 (50.6)	44 (49.4)		
Other	24	10 (41.7)	14 (58.3)		
WHO grade					
Low-grade (I + II)	79	29 (36.7)	50 (63.3)	11.289	0.001[b]
High-grade (III + IV)	116	71 (61.2)	45 (38.8)		
Invasion into surrounding tissue					
Yes	55	35 (63.6)	20 (36.4)	4.68	0.031[a]
No	140	65 (46.4)	75 (53.6)		

[a]P<0.05; [b]P<0.01. WHO, World Health Organization.

than that of patients with low NQO1 expression in ACC, bladder urothelial carcinoma, GBM, kidney renal clear cell carcinoma, rectum adenocarcinoma, skin cutaneous melanoma and UVM (Fig. 1H). Conversely, the survival of patients with prostate adenocarcinoma and high NQO1 expression was significantly longer than that of patients with low NQO1 expression. These results indicated that the high expression of NQO1 predicted the poor prognosis of patients with cancer and may be used as an important biomarker of cancer.

NQO1 expression is closely associated with MES subtype and adverse outcomes of GBM. It is well known that homologous recombination deficiency (HRD) and tumor mutational burden (TMB) are closely related to the choice of clinical treatment of cancer (23). Further studies showed that the expression of NQO1 was significantly correlated with ploidy, mutant-allele tumor heterogeneity (MATH), purity, HRD and TMB in most tumors (Fig. 2A). Through the intersection analysis of the aforementioned groups, the two negatively correlated members were obtained by Venn diagram: GBM and acute myeloid leukemia (AML) (Fig. 2B). These results indicated that NQO1 was closely related to the choice of clinical treatment of various types of cancer, but was not related to GBM and LAML. Subsequently, the present study further analyzed the relationship between NQO1 and the molecular subtype of cancer, and revealed that NQO1 mRNA expression had a significantly positive correlation with the subtype of GBM, but was not related to LAML (Fig. 2C). Therefore, the present

study focused on the molecular mechanism of NQO1 in GBM. The GSCA database showed that the mRNA expression of NQO1 was lower in the classical subtype of GBM than in the neural subtype (P<0.001). In particular, the mRNA expression of NQO1 was higher in the MES subtype than in the classical subtype of GBM, but no statistical significance was detected in the MES subtype compared with the neural and PN subtypes (Fig. 2D). These results suggested that NQO1 may be closely related to the malignant degree of GBM and could be a new target for identifying molecular subtypes of GBM.

Additionally, GES4536 and the Oncomine portal showed that NQO1 mRNA was upregulated in GBM tissues compared with that in normal brain tissues (Fig. 2E and F). To detect the expression level of NQO1 in GBM, IHC staining for NQO1 was conducted using a GBM tissue array containing 195 cases of GBM specimens and 24 cases of adjacent non-tumor specimens. High NQO1 expression was found in 100 of 195 (51.28% of cases with a score ≥4) GBM specimens compared with only 7 of 29 (24.14%) adjacent non-tumor specimens (Fig. 2G). IHC staining of NQO1 in representative GBM and adjacent non-tumor specimens is shown in Fig. 2H; the positive staining of NQO1 was observed mainly in the cytoplasm of cancer cells. As summarized in Table I, high NQO1 expression was significantly associated with high tumor grade (III + IV; P=0.001) and invasion (P=0.031), but was not significantly associated with age, sex, tumor size or tumor location (P>0.05). Further prognostic analysis indicated that high expression of NQO1 (high n=9) was associated with a shorter survival compared with low
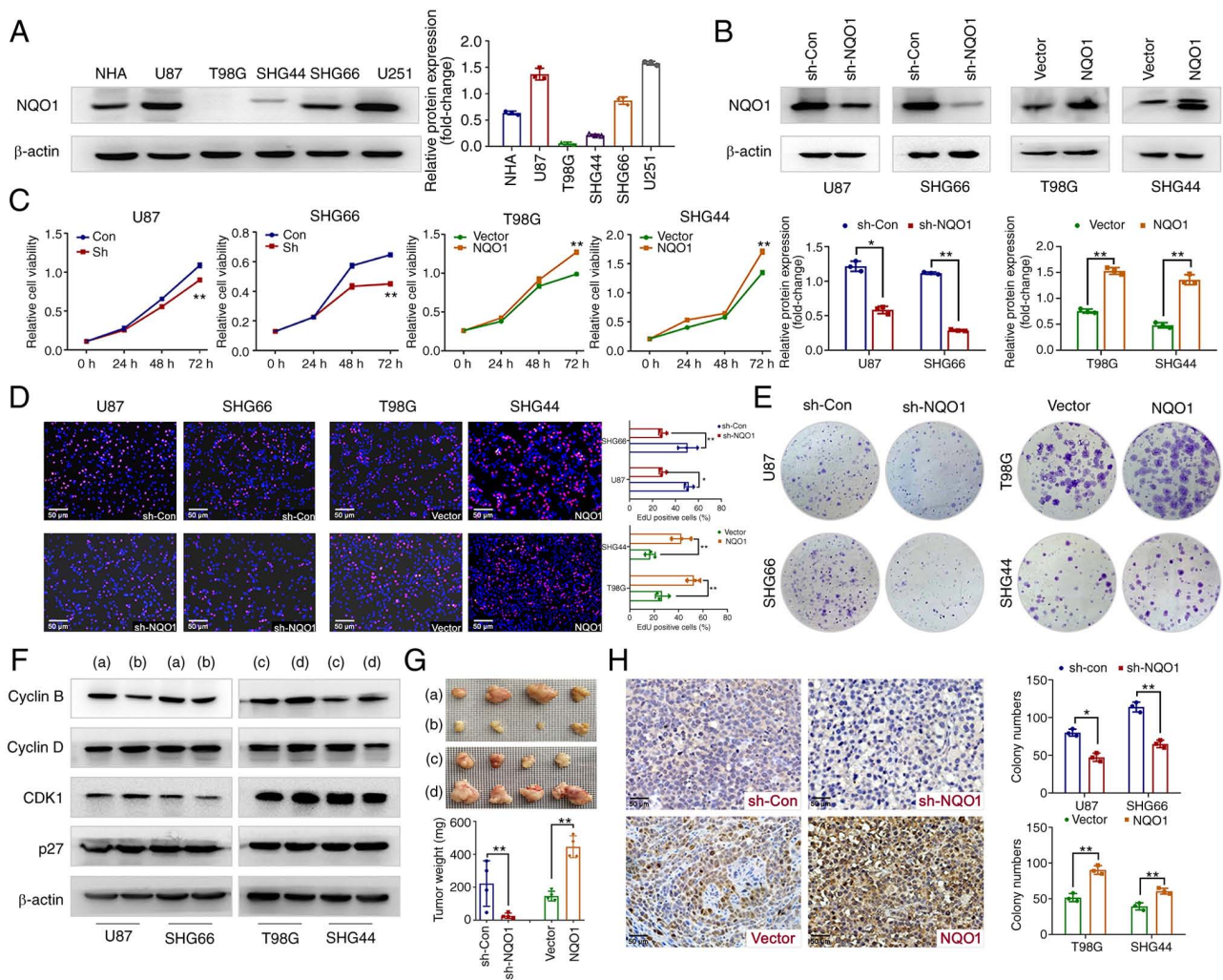
Figure 3. NQO1 regulates GBM cell proliferation *in vitro* and *in vivo*. (A) Expression levels of NQO1 in NHA and GBM cell lines were detected by western blotting. (B) Confirmation of NQO1 knockdown and overexpression were detected by western blotting in the sh-Con, sh-NQO1, vector and NQO1 overexpression groups. β-actin was used as a loading control. Effects of NQO1 on GBM cell proliferation were determined using (C) MTT, (D) EdU and (E) colony formation assays. Scale bar: 50 μm. (F) Expression levels of cell cyclin-related proteins in the NQO1 knockdown or overexpression groups were detected by western blotting. (a) sh-Con group, (b) shNQO1 group, (c) vector group (d) NQO1 overexpression group. (G) Representative images of GBM cell xenograft tumors in the four groups of nude mic. . (a) sh-Con group, (b) shNQO1 group, (c) vector group (d) NQO1 overexpression group. Xenograft tumor weights are shown (n=4/group). In the images, each grid represents 1x1 mm. (H) Ki67 expression in tumor sections were determined by immunohistochemical analysis. Scale bar: 50 μm. In all panels, t-tests for independent means were used for two group comparisons. *P<0.05, **P<0.01. NQO1, NAD(P)H:quinone acceptor oxidoreductase 1; NHA, normal human astrocytes; GBM, glioblastoma multiforme; sh, short hairpin; Con, control; CDK1, cyclin-dependent kinase 1.

expression of NQO1 (low n=65) in GBM based on database 201467_s_at (Fig. 2I). The diagnostic value was assessed using the ROC curve analysis in GBM, and the area under curve was 0.76 at 1 year, 0.72 at 3 years and 0.67 at 5 years, respectively (Fig. 2J). These findings suggested that NQO1 could be a prognostic marker for the MES subtype of GBM.

NQO1 participates in GBM cell proliferation in vivo and in vitro. To determine the biological function of NQO1 in GBM progression, the expression levels of NQO1 were detected in NHA and GBM cell lines. As shown in Fig. 3A, NQO1 was highly expressed in U87 (MES subtype), SHG66 (MES subtype), NHA and U251 cells, meanwhile it was lowly expressed in T98G (PN subtype) and SHG44 (PN subtype) cells. Therefore, U87 and SHG66 cells were chosen for NQO1 knockdown, and T98G and SHG44 cells were chosen for NQO1 overexpression. The transfection efficacy was verified using western blotting (Fig. 3B). Subsequently, MTT and EdU

assays revealed that NQO1 knockdown markedly inhibited cell proliferation and the percentage of EdU-positive cells, whereas NQO1 overexpression cells had the opposite effects (Fig. 3C and D). As expected, silencing NQO1 resulted in the formation of fewer and smaller colonies, whereas NQO1 overexpression enhanced clonogenicity (Fig. 3E).

Consistent with these observations, knockdown of NQO1 significantly reduced the expression levels of the G_2 phase marker Cyclin B; the opposite effects were obtained in cells overexpressing NQO1 (Figs. 3F and S1). Notably, there was no marked alterations in the protein expression levels of Cyclin D, CDK1 and p27 (Figs. 3F and S1). Subsequently, the *in vivo* experiment further confirmed the effect of NQO1 on tumorigenesis. The results revealed that NQO1 knockdown decreased tumor size and weight, whereas NQO1 overexpression had the opposite effects in a nude mouse model of subcutaneous tumors (Fig. 3G). In addition, NQO1 knockdown decreased the tumor size of intracranial tumors (Fig. S2). IHC staining of
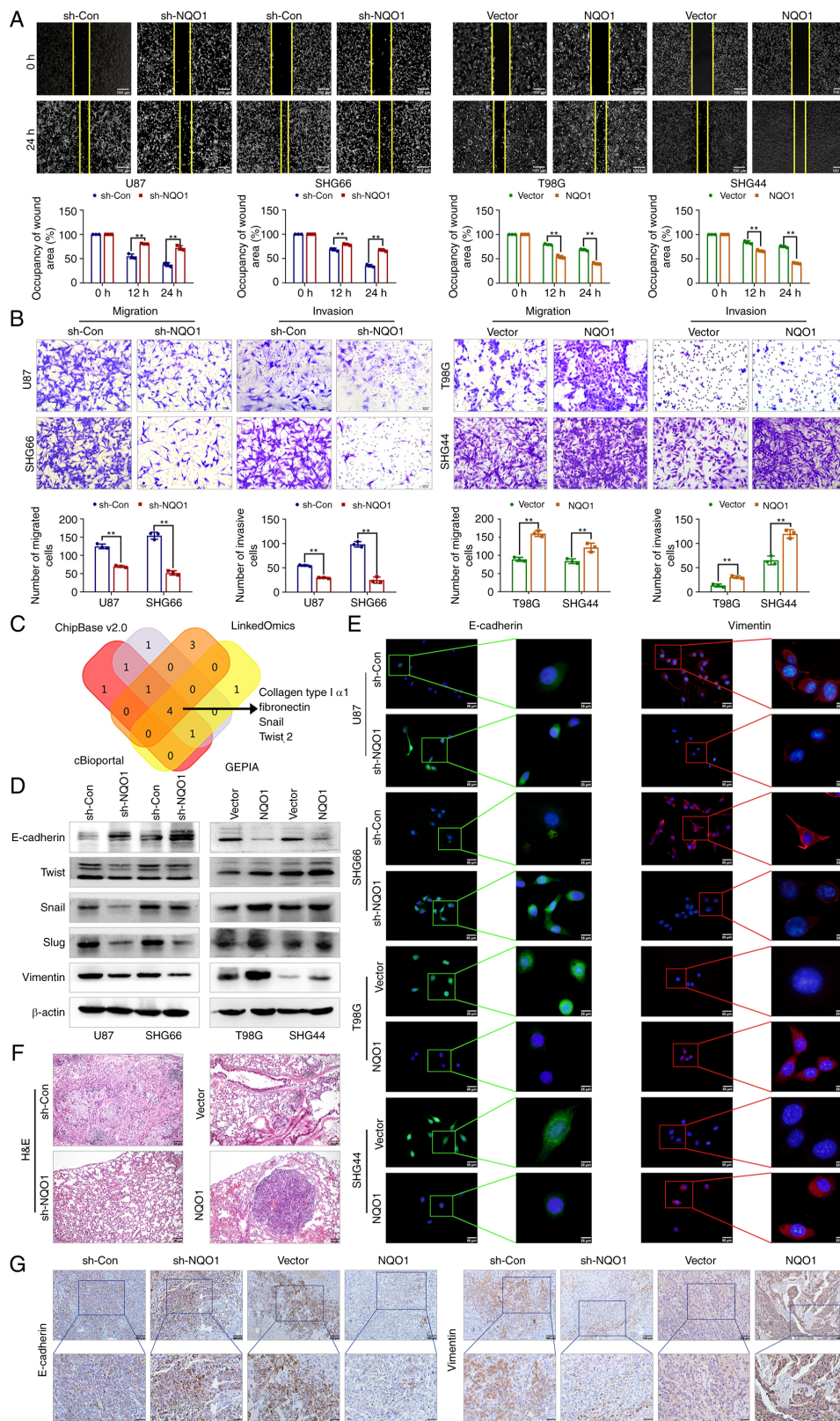
Figure 4. NQO1 accelerates GBM cell metastasis via the EMT process *in vitro* and *in vivo*. (A) Representative images of wound healing at 0 and 24 h after wound scratch in the sh-Con, sh-NQO1, vector and NQO1 overexpression groups. Wound healing percentage was quantified as width at 24 h/width at 0 h using ImageJ. Scale bar: 50 μm. (B) Representative images and quantification of the Transwell (migration and invasion) assays in the four groups of GBM cells. Scale bar: 50 μm. (C) Association between NQO1 expression and EMT markers in GBM were presented by using Venn diagram. The data were obtained from GEPIA, LinkOmics, CHIPbase and cBioportal database. (D) Expression levels of EMT markers were detected using western blotting in the four groups of GBM cells. β-actin was used as a loading control. Expression levels of EMT markers (E-cadherin and Vimentin) in the four groups of GBM cells were detected using immunofluorescence staining. Scale bar: 50 μm (right), 25 μm (left). Red staining indicates Vimentin, green staining indicates E-cadherin, blue staining indicates DAPI. (F) Representative images of H&E staining of the lung tissues. Scale bar: 100 μm. (G) Expression levels of E-cadherin and Vimentin in the four groups of xenograft tumor tissues were detected using immunohistochemical staining. Scale bars, upper: 100 μm; lower: 50 μm. **P<0.01. NQO1, NAD(P)H:quinone acceptor oxidoreductase 1; EMT, epithelial-mesenchymal transition; GBM, glioblastoma multiforme; sh, short hairpin; Con, control; HE, hematoxylin and eosin; Twist, twist-related protein; GEPIA, Gene Expression Profiling Interactive Analysis.
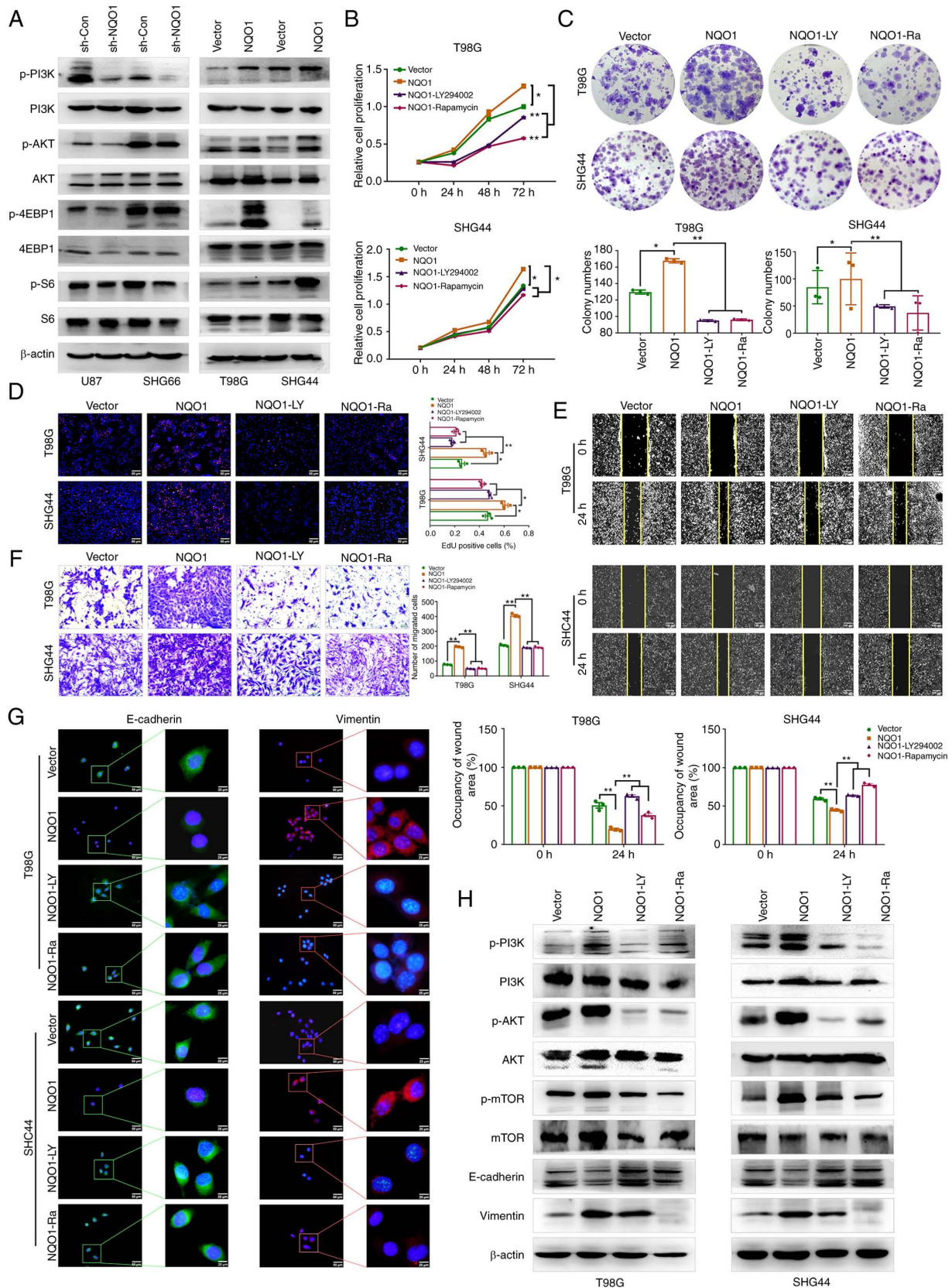
Figure 5. NQO1 activates the PI3K/Akt/mTOR pathway to regulate cell proliferation, movement and the EMT process. (A) Expression of PI3K/Akt/mTOR pathway markers was detected by western blotting in the four groups of GBM cells. β-actin was used as the loading control. Effects of LY294002 and Rapamycin on the proliferation of NQO1-overexpressing cells were detected using (B) MTT, (C) colony formation and (D) EdU assays. Effects of LY294002 and Rapamycin on the mobilty of NQO1-overexpressing cells were determined using (E) wound healing (scale bar: 50 μm) and (F) Transwell assays (scale bar: 25 μm). (G) Expression levels of EMT markers (E-cadherin and Vimentin) in the four groups of GBM cells were detected using immunofluorescence staining. Scale bar: 50 μm (right), 25 μm (left). Red staining indicates Vimentin, green staining indicates E-cadherin, blue staining indicates DAPI. (H) Expression levels of EMT markers and PAM pathway markers were detected using western blotting in the four groups of GBM cells. β-actin was used as a loading control. *P<0.05, **P<0.01. NQO1, NAD(P)H:quinone acceptor oxidoreductase 1; EMT, epithelial-mesenchymal transition; GBM, glioblastoma multiforme; sh, short hairpin; Con, control; p-, phosphorylated; 4EBP1, eIF4E-binding protein; S6, ribosomal protein S6; mTOR, mammalian target of rapamycin.

tumor tissue sections showed that Ki67 proliferation indexes were decreased in the NQO1 knockdown group and increased in the NQO1 overexpression group (Fig. 3H). These results indicated that NQO1 participated in GBM cell proliferation *in vivo* and *in vitro*.

NQO1 promotes cell migration and invasion, and induces the EMT. Subsequently, the present study focused on the functionalities of NQO1 in the metastatic potential of GBM cells. As expected, NQO1 significantly regulated the lateral and longitudinal migration, and invasion of GBM cells, as determined by wound healing and Transwell assays (Fig. 4A and B). Publicly available data (GEPIA, LinkOmics, CHIPbase and cBioportal database) predicted that the mRNA expression of NQO1 was positively correlated with collagen type I α1, fibronectin, Snail and Twist 2 (Fig. 4C). Consistent with this prediction, the results of western blotting showed that the epithelial marker E-cadherin was upregulated in NQO1 knockdown cells, whereas MES markers (Twist, Snail, Slug and Vimentin) were downregulated, whereas NQO1 overexpression had the opposite effects (Fig. 4D). Additionally, the present findings were further verified using IF staining (Fig. 4E). Similarly, *in vivo* metastasis analysis confirmed that knockdown of NQO1 significantly inhibited lung metastasis (Figs. 4F and S3), alongside a notable reduction in Vimentin and a promotion in E-cadherin in xenograft tissue sections (Fig. 4G). Taken together, these data indicated that NQO1 regulated EMT progression and metastasis in GBM.

Inhibitors of the PI3K/Akt/mTOR signaling pathway reverse the effects of NQO1 on GBM cell malignant phenotype. MES subtype-specific prognostic genes of GBM are mainly related to MES cell movement and the PI3K/Akt pathway (24). To assess whether NQO1 serves a role in GBM via the PI3K/Akt pathways, the expression of pathway markers in GBM cells was first detected by western blotting. The results revealed that silencing NQO1 could downregulate the protein expression levels of p-Akt/AKT, p-4EBP1/4EBP1 and p-S6/S6, and the opposite results were revealed in cells with NQO1 overexpression (Fig. 5A). Treatment with LY294002 (PI3K inhibitor) and Rapamycin (mTOR inhibitor) was used to further clarify the regulatory mechanism of the PI3K/Akt/mTOR signaling pathway in GBM. A series of rescue experiments showed that LY294002 and Rapamycin reversed the effects of NQO1 on the proliferation, colony formation and migration of GBM cells (Fig. 5B-F). Meanwhile, the fluorescence intensity of E-cadherin was increased, and that of Vimentin was decreased in the presence of both inhibitors (Fig. 5G). Western blotting results confirmed that LY294002 and Rapamycin weakened the effects of NQO1 on the EMT of GBM cells (Fig. 5H). These results suggested that NQO1 could induce malignant evolution of GBM by activating the PI3K/Akt/mTOR signaling pathway.

NQO1 promotes the malignant progression of GBM cells via Snail-dependent activation of the PI3K/Akt/mTOR pathway. Wang *et al* (25) reported that NQO1 promoted EMT, mainly by regulating Snail in hepatocellular carcinoma. Therefore, we hypothesized that NQO1 may accelerate EMT through Snail in GBM cells. To access this hypothesis, the correlation between NQO1 and Snail was predicted using a CHIPBase v3.0 database.

Spearman correlation analysis revealed that the mRNA expression levels of NQO1 were most associated with Snail (Fig. 6A). Subsequently, the potential binding interaction between NQO1 and Snail was identified using co-IP and colocalization IF assays (Fig. 6B and C). The ubiquitylation assay revealed that the ubiquitylation of Snail was markedly decreased in cells overexpressing NQO1, compared with the vector group cells, indicating that NQO1 could inhibit Snail degradation by regulating its ubiquitylation (Fig. 6D). Therefore, the present study investigated whether NQO1 overexpression promoted the process of GBM via Snail. To verify the hypothesis, NQO1-overexpressing cells were cocultured with three Snail siRNA sequences (si-Snail#1, si-Snail#2 and si-Snail#3) (Fig. S4). According to the knockdown effects of the siRNAS, si-Snail#2 and si-Snail#3 were used in subsequent experiments (Fig. 6E). As expected, colony formation assays indicated that Snail knockdown could reduce the proliferation of GBM cells induced by NQO1 overexpression (Fig. 6F). Similarly, wound healing and Transwell assays revealed that Snail knockdown decreased the migration of GBM cells compared with that in cells overexpressing NQO1 (Fig. 6G and H). Furthermore, the expression levels of PI3K/Akt/mTOR pathway markers and EMT-related markers were markedly decreased in si-Snail cells, as determined by western blotting (Fig. 6I). Taken together, Snail may be a potential effector of NQO1 in the regulation of GBM cell proliferation, migration, EMT and PI3K/Akt/mTOR signaling.

Discussion

NQO1 is upregulated in various types of cancer and is closely related to the poor prognosis of patients. The present study revealed that NQO1 was upregulated in GBM tissues and cells, especially in the MES subtype. Therefore, the present study proposed that NQO1 has an effect on the aggressiveness and development of GBM. However, the specific nature of the relationship between NQO1 expression and GBM classification warrants further study. By analyzing the relationship between NQO1 and clinical characteristics, significant differences in histological grade and tissue infiltration were revealed, which is consistent with the findings of a previous study (15,26). Furthermore, survival curve and ROC curve analyses showed a significant difference in the prognosis between patients with GBM who exhibited high NQO1 expression and those who exhibited low NQO1 expression. Therefore, NQO1 was indicated as a potential biomarker for assessing patients with GBM at higher risk of tumor invasion and/or metastasis.

Previous studies confirmed that NQO1 is a key molecular switch, and is associated with poor differentiation and metastasis of cancer cells (19,27). It was thus a logical hypothesis that NQO1 was involved in GBM invasion and development. To authenticate this hypothesis, a series of biological experiments was employed to investigate the role of NQO1 in regulating the invasion and proliferation of GBM cells. The results demonstrated that NQO1 knockdown inhibited cell proliferation, invasion and EMT in GBM cells, whereas NQO1 overexpression had the opposite effect. Furthermore, NQO1 overexpression led to a significant increase in tumor formation and metastasis, as determined in *in vivo* experiments. Notably, our previous study similarly showed that NQO1 overexpression promoted cell mobility and EMT in BC cells (19). These
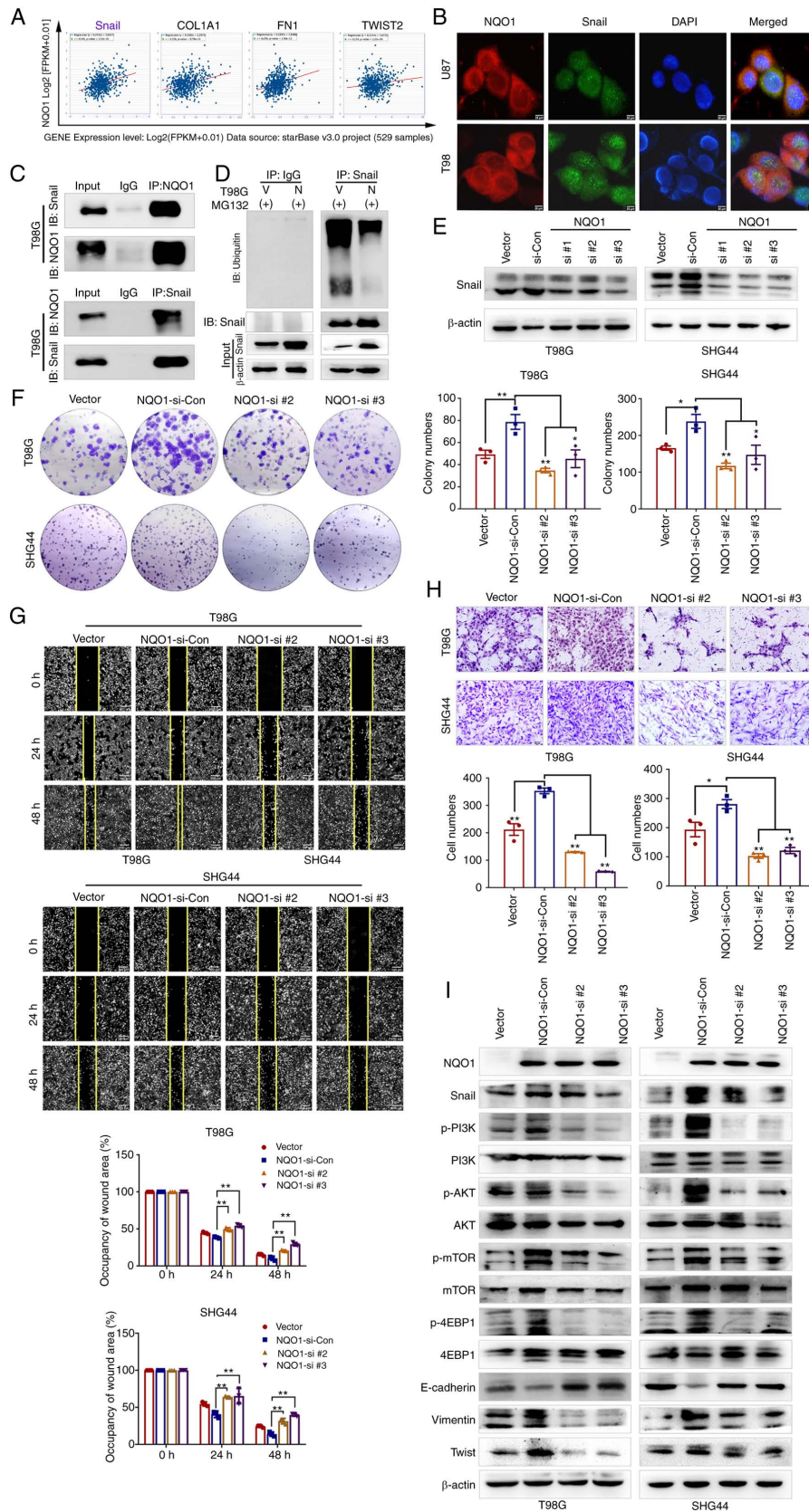
Figure 6. NQO1/Snail regulates GBM progression by activating the PI3K/Akt/mTOR signaling pathway. (A) Correlations between NQO1 expression, and Snail, COL1A1, FN1 and TWIST2 were analyzed using the ENCORI database. (B) Colocalization phenomena of NQO1 and Snail in GBM cells was confirmed using immunofluorescence analysis. Scale bar: 25 μm. (C) Interaction of NQO1 and Snail protein in GBM cells was analyzed using co-IP. (D) T98G cells of the vector and NQO1 overexpression groups were treated with 10 μM MG132 for 6 h. The ubiquitination of Snail was examined by western blotting. (E) Snail expression in GBM cells in the Vector group, and in those co-transfected with NQO1 and si-Con or siSnail (si #1, si #2 and si #3), as determined using western blotting. (F) Proliferation of T98G and SHG44 cells were measured by colony formation assay. Migration of cells was determined using (G) wound healing (scale bar: 50 μm) and (H) Transwell assays (scale bar: 25 μm). (I) Expression levels of epithelial-mesenchymal transition markers and PI3K/Akt/mTOR pathway markers were detected using western blotting. β-actin was used as the loading control. *P<0.05, **P<0.01. NQO1, NAD(P)H:quinone acceptor oxido-reductase 1; GBM, glioblastoma multiforme; si, small interfering; Con, control; IP, immunoprecipitation; IB, immunoblot; V, Vector; N, NQO1.
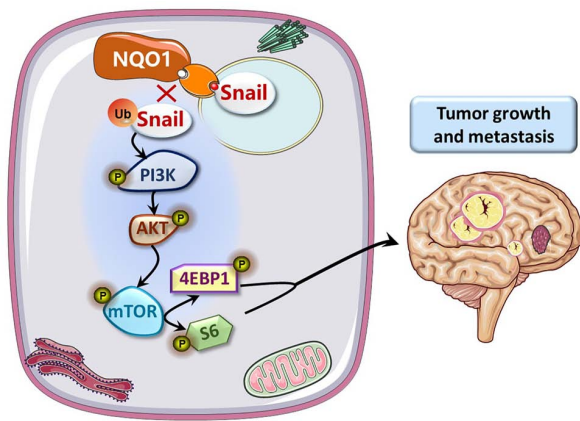
Figure 7. Mechanistic diagram depicting the role of NQO1 in GBM cell aggressiveness via the PI3K/Akt/mTOR/Snail pathway. NQO1 could promote GBM aggressiveness by activating the PI3K/Akt/mTOR signaling pathway via blocking Snail degradation. NQO1, NAD(P)H:quinone acceptor oxidoreductase 1; GBM, glioblastoma multiforme; 4EBP1, eIF4E-binding protein; S6, ribosomal protein S6; mTOR, mammalian target of rapamycin.

results support the hypothesis that NQO1 is an important factor in judging the aggressiveness of GBM cells.

A previous study suggested that NQO1 influences the aggressiveness of different human tumor cells through various signaling pathways (28). Zhou *et al* (29) reported that NQO1 promotes the proliferation of hepatocellular carcinoma cells via the SIRT6/AKT/XIAP signaling pathway (20). Attenuation of NQO1 has also been reported to aggravate prostate cancer and tumor cell plasticity through activating TGF-β signaling (20). It is widely known that the PI3K/Akt pathway regulates cell proliferation, aggressiveness and metabolism in multiple types of cancer, especially in GBM (30,31). Suppression of the PI3K/Akt pathway may be crucial to block metastasis in GBM (32,33). It has been reported that NQO1 promotes the expression of PI3K and AKT signaling pathways through TNF (34). Therefore, the present study investigated whether NQO1 was involved in the PI3K/Akt pathway in GBM cells. The results revealed that NQO1 may be an important activator of the PI3K/Akt/mTOR pathway, and PI3K/Akt/mTOR inhibitors (LY294002 and Rapamycin) reduced the proliferation, invasion and EMT in NQO1-overexpressing cells *in vitro*. Taken together, these results indicated that NQO1 may induce EMT via the PI3K/Akt/mTOR pathway in GBM cells.

The PI3K/Akt/mTOR signaling pathway, one of the most critical intracellular signaling pathways, can regulate metastasis via EMT markers, such as Vimentin and Snail (35,36). AKT-induced long noncoding RNA VAL has been shown to promote EMT-independent metastasis through Vimentin degradation (37). Inhibition of the LASP1/PI3K/AKT/Snail signaling pathway may reduce tumor progression in GBM cells (38). Moreover, it has been reported that NQO1 plays a crucial role in mediating EMT by activating Snail in postmitotic corneal cells, thus conducing to Fuchs endothelial corneal dystrophy (39). Our previous study confirmed that NQO1 could promote hepatocellular carcinoma progression and metastasis by regulating Snail stability (25). The present study revealed that NQO1 promoted EMT by blocking proteasome degradation of Snail. We also indicated that the NQO1-activated PI3K/Akt/mTOR pathway drives EMT-dependent metastasis in GBM cells

through Snail degradation. These results suggested that NQO1 could influence Snail stability via ubiquitylation, and NQO1 could regulate the proliferation and EMT of GBM cells via the PI3K/Akt/mTOR/Snail signaling pathway (Fig. 7).

In conclusion, the present study identified that upregulation of NQO1 may be critical for the acquired GBM aggressive phenotype, and demonstrated that it was associated with the poor prognosis of patients with GBM. Additionally, NQO1 may drive GBM cell proliferation and invasion through EMT via the PI3K/Akt/mTOR/Snail pathway. This study indicated that NQO1 could be used as a diagnostic biomarker or therapeutic target of GBM, especially the MES subtype.

Acknowledgements

Funding

Availability of data and materials

The datasets used and/or analyzed during the current study are available from the corresponding author on reasonable request.

Authors' contributions

LZ, SPY and CHQ confirmed the authenticity of all the raw data, conceived this study and take responsibility for the quality of the data. YY participated in analysis and interpretation of data, and prepared all figures. RX and JSQ participated in the tissue sample selection and experiments. CHQ and ZHL acquired data and played an important role in interpreting the results. LZ, SPY and CHQ performed the data analysis and wrote the manuscript. All authors read and approved the final manuscript.

Ethics approval and consent to participate

The use of the glioma tissue microarray in this research was approved by the Ethics Committee of Yanbian University Medical College (approval no. YD20230406015) and was conducted in compliance with the tenets of The Declaration of Helsinki. The requirement for ethics approval for the use of primary cell lines was waived. All animal experiments were performed in accordance with the procedures and protocols of the Laboratory Animal Center of Yanbian University.

Patient consent for publication

Not applicable.

Competing interests

The authors declare that they have no competing interests.

References

1. Siegel RL, Miller KD, Fuchs HE and Jemal A: Cancer statistics, 2022. CA Cancer J Clin 72: 7-33, 2022.
2. Fang R, Chen X, Zhang S, Shi H, Ye Y, Shi H, Zou Z, Li P, Guo Q, Ma L, et al: EGFR/SRC/ERK-stabilized YTHDF2 promotes cholesterol dysregulation and invasive growth of glioblastoma. Nat Commun 12: 177, 2021.
3. Chan DT, Hsieh SY, Kam MK, Cheung TCY, Ng SCP and Poon WS: Pattern of recurrence and factors associated with cerebrospinal fluid dissemination of glioblastoma in Chinese patients. Surg Neurol Int 7: 92, 2016.
4. Verhaak RG, Hoadley KA, Purdom E, Wang V, Qi Y, Wilkerson MD, Miller CR, Ding L, Golub T, Mesirov JP, et al: Integrated genomic analysis identifies clinically relevant subtypes of glioblastoma characterized by abnormalities in PDGFRA, IDH1, EGFR, and NF1. Cancer Cell 17: 98-110, 2010.
5. Wang Z, Shi Y, Ying C, Jiang Y and Hu J: Hypoxia-induced PLOD1 overexpression contributes to the malignant phenotype of glioblastoma via NF-κB signaling. Oncogene 40: 1458-1475, 2021.
6. Li Y, Wang X, Qi S, Gao L, Huang G, Ren Z, Li K, Peng Y, Yi G, Guo J, et al: Spliceosome-regulated RSRP1-dependent NF-κB activation promotes the glioblastoma mesenchymal phenotype. Neuro Oncol 23: 1693-1708, 2021.
7. Tang G, Luo L, Zhang J, Zhai D, Huang D, Yin J, Zhou Q, Zhang Q and Zheng G: lncRNA LINC01057 promotes mesenchymal differentiation by activating NF-κB signaling in glioblastoma. Cancer Lett 498: 152-164, 2021.
8. Amicone L, Marchetti A and Cicchini C: Exosome-associated circRNAs as key regulators of EMT in cancer. Cells 11: 1716, 2022.
9. Liu Y, Guo G, Lu Y, Chen X, Zhu L, Zhao L, Li C, Zhang Z, Jin X, Dong J, et al: Silencing IKBKE inhibits the migration and invasion of glioblastoma by promoting Snail1 degradation. Clin Transl Oncol 24: 816-828, 2022.
10. Yun EJ, Kim D, Hsieh JT and Baek ST: Stanniocalcin 2 drives malignant transformation of human glioblastoma cells by targeting SNAI2 and matrix Metalloproteinases. Cell Death Discov 8: 308, 2022.
11. Zhong C, Li X, Tao B, Peng L, Peng T, Yang X, Xia X and Chen L: LIM and SH3 protein 1 induces glioma growth and invasion through PI3K/AKT signaling and epithelial-mesenchymal transition. Biomed Pharmacother 116: 109013, 2019.
12. Nan Y, Guo L, Lu Y, Guo G, Hong R, Zhao L, Wang L, Ren B, Yu K, Zhong Y and Huang Q: miR-451 suppresses EMT and metastasis in glioma cells. Cell Cycle 20: 1270-1278, 2021.
13. Ernster L and Lindberg O: Animal mitochondria. Annu Rev Physiol 20: 13-42, 1958.
14. Yadav U, Kumar P and Rai V: NQO1 gene C609T polymorphism (dbSNP: rs1800566) and digestive tract cancer risk: A meta-analysis. Nutr Cancer 70: 557-568, 2018.
15. Yang Y, Zhang Y, Wu Q, Cui X, Lin Z, Liu S and Chen L: Clinical implications of high NQO1 expression in breast cancers. J Exp Clin Cancer Res 33: 14, 2014.
16. Li Z, Zhang Y, Jin T, Men J, Lin Z, Qi P, Piao Y and Yan G: NQO1 protein expression predicts poor prognosis of non-small cell lung cancers. BMC Cancer 15: 207, 2015.
17. Lin L, Sun J, Tan Y, Li Z, Kong F, Shen Y, Liu C and Chen L: Prognostic implication of NQO1 overexpression in hepatocellular carcinoma. Hum Pathol 69: 31-37, 2017.
18. Madajewski B, Boatman MA, Chakrabarti G, Boothman DA and Bey EA: Depleting tumor-NQO1 potentiates anoikis and inhibits growth of NSCLC. Mol Cancer Res 14: 14-25, 2016.
19. Yang Y, Zhu G, Dong B, Piao J, Chen L and Lin Z: The NQO1/PKLR axis promotes lymph node metastasis and breast cancer progression by modulating glycolytic reprogramming. Cancer Lett 453: 170-183, 2019.
20. Thapa D, Huang SB, Muñoz AR, Yang X, Bedolla RG, Hung CN, Chen CL, Huang THM, Liss MA, Reddick RL, et al: Attenuation of NAD[P]H:quinone oxidoreductase 1 aggravates prostate cancer and tumor cell plasticity through enhanced TGFβ signaling. Commun Biol 3: 12, 2020.
21. Shimokawa M, Yoshizumi T, Itoh S, Iseda N, Sakata K, Yugawa K, Toshima T, Harada N, Ikegami T and Mori M: Modulation of Nqo1 activity intercepts anoikis resistance and reduces metastatic potential of hepatocellular carcinoma. Cancer Sci 111: 1228-1240, 2020.
22. Wu W, Klockow JL, Zhang M, Lafortune F, Chang E, Jin L, Wu Y and Daldrup-Link HE: Glioblastoma multiforme (GBM): An overview of current therapies and mechanisms of resistance. Pharmacol Res 171: 105780, 2021.
23. Liu YL, Selenica P, Zhou Q, Iasonos A, Callahan M, Feit NZ, Boland J, Vazquez-Garcia I, Mandelker D, Zehir A, et al: BRCA Mutations, homologous DNA repair deficiency, tumor mutational burden, and response to immune checkpoint inhibition in recurrent ovarian cancer. JCO Precis Oncol 4: PO.20.00069, 2020.
24. Shahcheraghi SH, Tchokonte-Nana V, Lotfi M, Lotfi M, Ghorbani A and Sadeghnia HR: Wnt/beta-catenin and PI3K/Akt/mTOR signaling pathways in glioblastoma: Two main targets for drug design: A review. Curr Pharm Des 26: 1729-1741, 2020.
25. Wang X, Liu Y, Han A, Tang C, Xu R, Feng L, Yang Y, Chen L and Lin Z: The NQO1/p53/SREBP1 axis promotes hepatocellular carcinoma progression and metastasis by regulating Snail stability. Oncogene 41: 5107-5120, 2022.
26. Begleiter A and Fourie J: Induction of NQO1 in cancer cells. Methods Enzymol 382: 320-351, 2004.
27. Pradubyat N, Sakunrangsit N, Mutirangura A and Ketchart W: NADPH: Quinone oxidoreductase 1 (NQO1) mediated anti-cancer effects of plumbagin in endocrine resistant MCF7 breast cancer cells. Phytomedicine 66: 153133, 2020.
28. Yang Y, Zheng J, Wang M, Zhang J, Tian T, Wang Z, Yuan S, Liu L, Zhu P, Gu F, et al: NQO1 promotes an aggressive phenotype in hepatocellular carcinoma via amplifying ERK-NRF2 signaling. Cancer Sci 112: 641-654, 2021.
29. Zhou HZ, Zeng HQ, Yuan D, Ren JH, Cheng ST, Yu HB, Ren F, Wang Q, Qin YP, Huang AL and Chen J: NQO1 potentiates apoptosis evasion and upregulates XIAP via inhibiting proteasome-mediated degradation SIRT6 in hepatocellular carcinoma. Cell Commun Signal 17: 168, 2019.
30. Precilla SD, Biswas I, Kuduvalli SS and Anitha TS: Crosstalk between PI3K/AKT/mTOR and WNT/β-Catenin signaling in GBM-could combination therapy checkmate the collusion? Cell Signal 95: 110350, 2022.
31. Courtney KD, Corcoran RB and Engelman JA: The PI3K pathway as drug target in human cancer. J Clin Oncol 28: 1075-1083, 2010.
32. Wojtas B, Gielniewski B, Wojnicki K, Maleszewska M, Mondal SS, Nauman P, Grajkowska W, Glass R, Schüller U, Herold-Mende C and Kaminska B: Gliosarcoma is driven by alterations in PI3K/Akt, RAS/MAPK pathways and characterized by collagen gene expression signature. Cancers (Basel) 11: 284, 2019.
33. Burris HA III: Overcoming acquired resistance to anticancer therapy: Focus on the PI3K/AKT/mTOR pathway. Cancer Chemother Pharmacol 71: 829-842, 2013.
34. Ahn YJ, Lim JW and Kim H: Docosahexaenoic acid induces expression of NAD(P)H: Quinone oxidoreductase and heme oxygenase-1 through Activation of Nrf2 in cerulein-stimulated pancreatic acinar cells. Antioxidants (Basel) 9: 1084, 2020.
35. Liang S, Guo H, Ma K, Li X, Wu D, Wang Y, Wang W, Zhang S, Cui Y, Liu Y, et al: A PLCB1-PI3K-akt signaling axis activates EMT to promote cholangiocarcinoma progression. Cancer Res 81: 5889-5903, 2021.
36. Lee S, Choi EJ, Cho EJ, Lee YB, Lee JH, Yu SJ, Yoon JH and Kim YJ: Inhibition of PI3K/Akt signaling suppresses epithelial-to-mesenchymal transition in hepatocellular carcinoma through the Snail/GSK-3/beta-catenin pathway. Clin Mol Hepatol 26: 529-539, 2020.
37. Tian H, Lian R, Li Y, Liu C, Liang S, Li W, Tao T, Wu X, Ye Y, Yang X, et al: AKT-induced lncRNA VAL promotes EMT-independent metastasis through diminishing Trim16-dependent Vimentin degradation. Nat Commun 11: 5127, 2020.
38. Zhong C, Chen Y, Tao B, Peng L, Peng T, Yang X, Xia X and Chen L: LIM and SH3 protein 1 regulates cell growth and chemosensitivity of human glioblastoma via the PI3K/AKT pathway. BMC Cancer 18: 722, 2018.
39. Katikireddy KR, White TL, Miyajima T, Vasanth S, Raoof D, Chen Y, Price MO, Price FW and Jurkunas UV: NQO1 downregulation potentiates menadione-induced endothelial-mesenchymal transition during rosette formation in Fuchs endothelial corneal dystrophy. Free Radic Biol Med 116: 19-30, 2018.